ISSN 1810-2328, Journal of Engineering Thermophysics, 2019, Vol. 28, No. 4, pp. 489–498. © Pleiades Publishing, Ltd., 2019.

Characterization of Multi-Jet Cooling Using High-Speed Visualization and IR Thermography

A. D. Nazarov[1,2*], N. V. Miskiv[1,2], A. S. Surtaev[1,2], and V. S. Serdyukov[1,2]

[1] *Kutateladze Institute of Thermophysics, Siberian Branch, Russian Academy of Sciences, pr. Akad. Lavrent'eva 1, Novosibirsk, 630090 Russia*

[2] *Novosibirsk State University, ul. Pirogova 2, Novosibirsk, 630090 Russia*

Received June 6, 2019; in final form, October 16, 2019; accepted October 17, 2019

Abstract—The paper presents the results of experimental study on characteristics of non-boiling multi-jet water cooling. Experimental data on the characteristics of droplet jets including the distribution of droplets sizes and their velocity, as well as liquid irrigation patterns on a transparent heating surface, were obtained using high-speed visualization. The surface temperature field of the thin-film ITO heater was measured using IR thermography. The usage of synchronized techniques revealed the relationship between the irrigation dynamics and the temperature field of the heating surface. Moreover, IR thermography made it possible to determine both the distribution of local heat transfer rate in various areas of the impact surface and the integral heat transfer during multi-jet cooling. In particular, the dependence of the integral heat transfer rate on the distance between the spray source and the heater was revealed and it was shown that there is an optimal configuration of liquid irrigation pattern at which the maximum heat transfer coefficient is observed.

DOI: 10.1134/S1810232819040040

INTRODUCTION

It is known that the use and utilization of energy in any process in the energy sector, industry (including the chemical one), and the housing and public utilities sector include the process of heat transfer. Technical and economic indicators of energy equipment are largely determined by parameters of heat exchangers. As the unit capacity of power plants increases, the absolute weight and size parameters of heat exchangers used in production increase too. Thus, one of the main trends in improving heat exchangers of various types is to enhance the effectiveness of their work and to reduce their size and metal content. Now spray/jet cooling, along with microchannel two-phase systems and heat pipes, is one of the most efficient methods of heat transfer. However, as compared with the above-described cooling systems, the scope of gas-droplet flows is much wider [1, 2]. In particular, in recent years, foreign literature offers more and more works aimed at creating new types of evaporative devices and cooling systems in which a heat transfer surface is watered by sprays and jets [3].

Today, the vast majority of experimental studies of heat transfer at spray and jet cooling involve measurements of integral thermal characteristics using thermocouples and local temperature sensors with low temporal and spatial resolutions. General data do not allow obtaining information on local characteristics of heat transfer, assessing their contribution to the integral heat transfer, and fully understanding the main mechanisms of heat transfer, which is very important for developing theoretical models for describing the process and engineering methods for calculating systems with spray/jet cooling.

In this paper, a measurement method based on high-speed synchronized infrared thermography and video recording was used to study the temperature field in relation to the process of formation and behavior of precipitated liquid on a heated surface. This method made it possible to obtain experimental data on the hydrodynamics of impact interaction of a jet-droplet flow of four jets with a heat-transfer surface and the related temperature fields of the surface. The dependences of the integral heat transfer of the heat-generating surface to the entire four jet-droplet flow and local heat transfer to one jet in the flow are presented for different distances from the flow source to the surface.

* E-mail: nazarov@itp.nsc.ru

EXPERIMENTAL SETUP

The experimental facility for the study of the spray hydrodynamic parameters and local and integral characteristics of heat transfer using a controlled multi-nozzle spraying source and individual nozzles of various types consists of four main parts. These parts are the hydrodynamic circuit for supplying liquid and gas, the jet flow source, the heating element, and the high-speed video/infrared camera (Figs. 1a and 1b).

The flow source, the heating assembly, and the high-speed cameras are mounted on carriers to the rail and are located on the same axis. This design enables easy variation of the distance from the spray source to the heater.

In the experiments, the Bosch EV14L nozzle was used (Fig. 2). The nozzle has four outlets with a diameter of 100 μm located at the vertices of a square with a side of 500 μm. The automated nozzle control system enables formation of both stationary and non-stationary droplet-jet flows (periodic irrigation) with given characteristics of the period and duration of the droplet-jet phase.

The working liquid was distilled water; the initial temperature of the liquid was ambient and varied in the range of 15–24°C. Figure 3 shows the dependence of the flow rate on the liquid pressure at the inlet. The liquid flow was measured by the volumetric method. The flow measurement error was 3%. The liquid flow rate G for the stationary irrigation regime varied in the range of 5.3–8.2 cm^3/s depending on the overpressure (1.5–3 atm).

The target was a sapphire substrate. A thin film heater of indium tin oxide ITO was deposited onto the backside of the substrate. The substrate with the thin film heater was sealed in plexiglass mounted

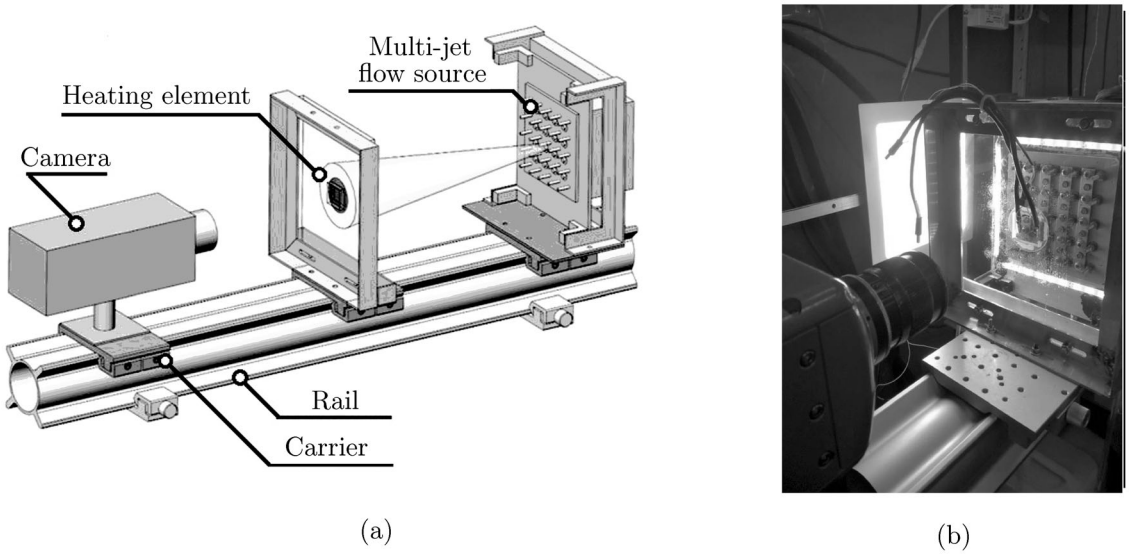

Fig. 1. (a) Scheme and (b) photo of experimental test bench with multi-nozzle source of jet spraying.

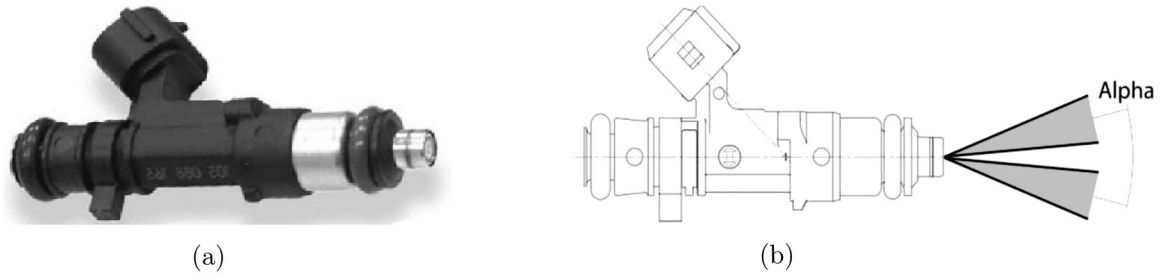

Fig. 2. Bosch EV14L nozzle; (a) photo, (b) diagram.

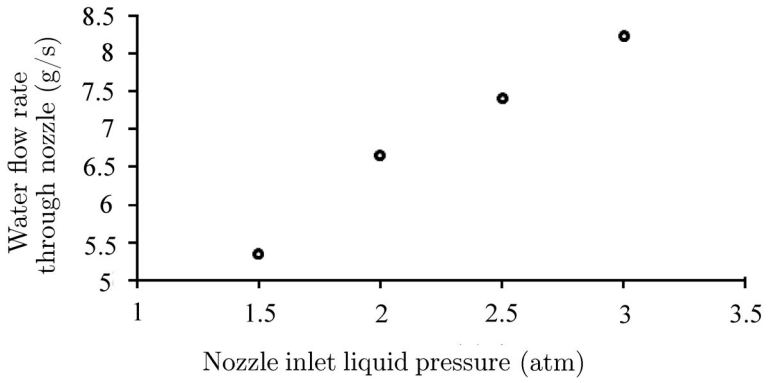

Fig. 3. Liquid flow rate vs. pressure at nozzle inlet.

in an aluminum frame. Samples were heated due to the Joule effect, using a DC power supply Elektro Automatik PS 8080-60 DT with thin silver electrodes vacuum deposited onto ITO film.

The heat flux density q was determined from the value of the current passed through the heater and the voltage drop on it. The relative error of the measurement of the heat flux in the experiments was 5%. In the experiments, a Phantom v.7.0 high-speed video camera was installed from the side of the multi-jet source opposite to the light source. Visualization by the shadow technique was performed with a frequency of up to $10 \cdot 10^3$ FPS and with a maximum resolution of 40 μm. To analyze the irrigation pattern of the working surface, high-speed visualization was performed on the reverse side of the transparent heat exchange surface with a recording frequency of up to $2 \cdot 10^3$ FPS. To measure the distribution of the temperature field of the impacted surface, a high-speed infrared (IR) FLIR Titanium HD 570 M camera was installed behind the target. IR recording was carried out with a frequency of 200 FPS and resolution of 88 μm.

For correct measurement of non-stationary temperature field of the impacted surface using a high-speed infrared camera, calibration experiments without liquid supply were performed in advance. For this purpose, the working surface was uniformly heated step by step to a temperature of about 75°C. The temperature field of the surface was recorded using the IR camera. A calibrated Honeywell resistance temperature detector located on the sapphire substrate monitored the recorded temperature. As a result of these experiments, calibration dependencies were obtained for correct measurement of the surface temperature field.

HEATING ELEMENT

A sapphire substrate with a diameter of 50 mm and a thickness of 400 μm with deposited film (1 μm thick; area of 4 cm^2) of indium tin oxide (ITO) was used as a heater. The main advantage of using ITO as a heater material in experiments at spray cooling is its transparency in the visible spectrum (380–750 nm) and opacity in the mid-IR spectrum (3–5 μm). This property makes it possible to measure a non-stationary temperature field on the ITO film surface with an infrared camera and visually record the dynamics of irrigation of heat transfer surface with a high-speed video camera. For this reason, such design of heating element was recently widely used for pool boiling experiments [4–6]. According to the manufacturer (Hong Yuan Wafer Tech Co), the surface roughness of the sapphire substrate was $Ra < 20$ nm. Morphological analysis of the samples was done using a Hitachi S-3400N scanning electron microscope. Analysis of the wetting properties of the heaters was done using the KRUSS DSA-100. The measurement results showed that for water the wetting angle on the sapphire surface was 60°.

PARAMETERS OF MULTI-JET FLOW

It is known that the intensity of heat transfer during spray cooling is influenced by spray parameters such as the size of the droplets, their velocity, and the character of irrigation of the impact surface [1]. Therefore, in the first stage, the shadow technique using a high-speed video camera Phantom v.7.0

was applied to determine the spray angle of the drop flow and the size of the liquid particles and their velocity against the distance from the source and the flow rate of the liquid. To do this, the camera was mounted on a tripod normally to the direction of flow and opposite a LED lamp. The visualization by the shadow method was performed with a frequency of up to 10 kHz and with a maximum resolution of up to 40 μm. The pictures (Fig. 4) present visualization of the propagation of the jet front from a single injector, obtained in the periodic pulsed regime ($P = 2$ atm). As can be seen from these pictures, such visualization enables determination of a lot of parameters of interest, such as the size of the droplets, their velocity, and the spray angle. Analysis of the data showed that the spray angle was practically independent of the liquid flow rate over the entire pressure range; its mean value was 6.5°. The obtained data make it easy to estimate the area of the impact surface against the distance between the multi-jet source and the target.

Figure 5 presents the size distribution of droplets at various pressures ($P = 2$ atm, $P = 3$ atm). All the measurements were carried out at distances exceeding the distance of instability development and disintegration of the jet into individual droplets. The analysis shows that the deviation of the droplet sizes d from the most probable value did not exceed 0.13 mm at $d_{av} = 0.4$–0.55 mm. Besides that, comparison of results obtained at different pressures showed that the mean droplet size decreased slightly with increasing overpressure.

Using the above-described shadow technique, the velocity of liquid droplets formed by a single nozzle was measured at various flow rates and distances from the jet source. Figure 6 demonstrates the character of the trajectory of individual droplets in the flow at different nozzle inlet pressures: 2 and 3.5 atm in the steady-state spraying regime. The technique was as follows. The coordinates of selected three droplets passing a distance of 40 mm were traced at different time moment. The diameter of the droplets was chosen close to the most probable diameter for each pressure (see Fig. 5). It can be seen from the data that the gravitational forces do not affect the trajectory of droplets passing a distance of

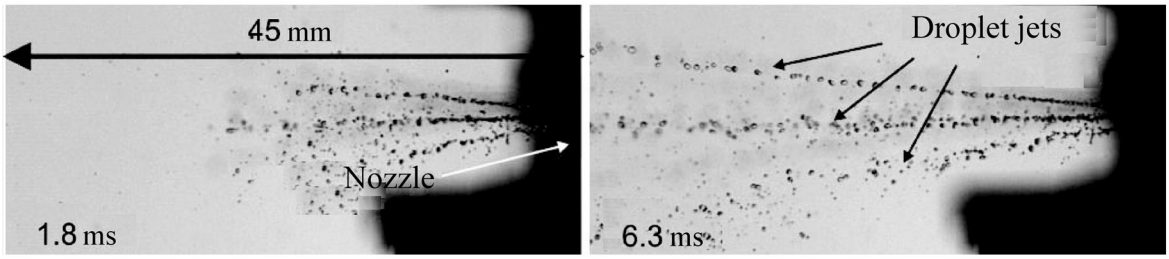

Fig. 4. Frames of high-speed video recording of process of propagation of droplet liquid jets from single injector at periodically pulsed regime ($P = 2$ atm).

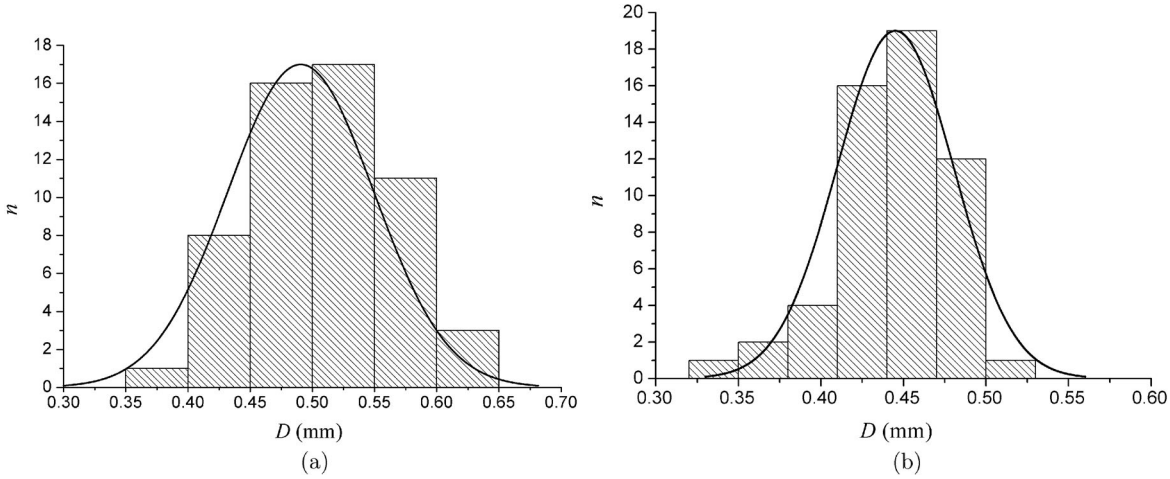

Fig. 5. Distribution of diameters of water droplets in flow formed by Bosch EV14L nozzle at various inlet pressures: (a) $P = 2$ atm, (b) $P = 3$ atm.

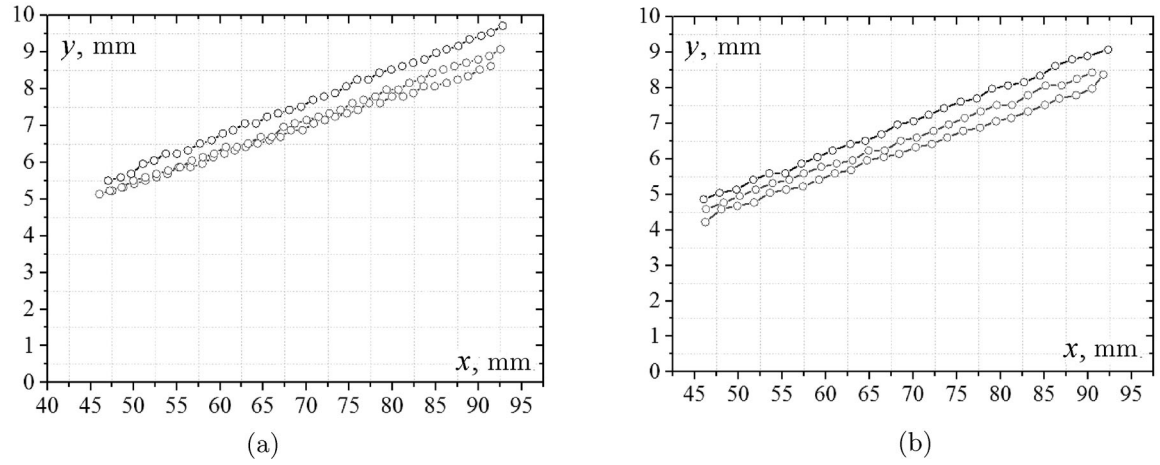

Fig. 6. Trajectories of three separate droplets moving from source at inlet overpressure of (a) 2 atm and (b) 3.5 atm.

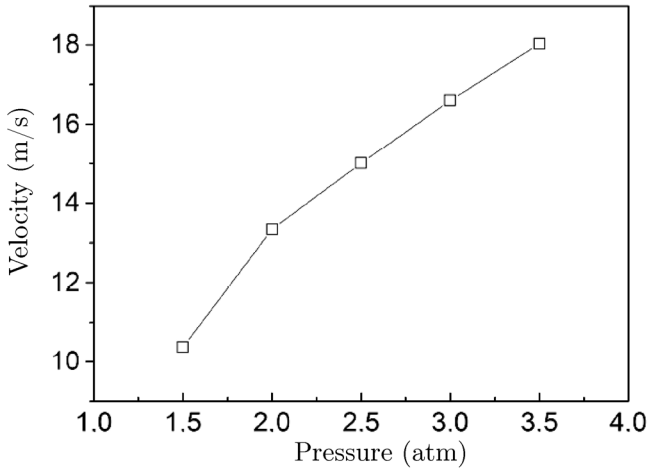

Fig. 7. Mean velocity of liquid droplets of various sizes vs. pressure at inlet of Bosch EV14L nozzle.

40 mm, and therefore the trajectory of the flow droplets is linear. Therefore, the velocity of the droplets is constant over time.

These data were used to obtain the dependence of the droplet velocity on the excess pressure (Fig. 7). Analysis of the resulting dependence shows that the droplet velocity substantially depends on the overpressure and reaches 18 m/s at $P = 3.5$ atm.

INTERACTION OF MULTI-JET FLOW WITH SURFACE

Figure 8 shows photographs of liquid flows occurring at impact of water jets with a source exit velocity $V_0 = 16.5$ m/s and a mass flow rate $G = 8.23$ g/s ($P = 3$ atm). The distance from the jet source to the target was varied as a parameter.

It can be seen from Fig. 8 that the liquid spreads from the centers of jet impacts over the surface in all directions. There is a film structure around the centers of the jet impacts with the border in the form of hydraulic ripple. It is obvious that the liquid film is thinner inside this circle, and its flow rate is higher than the same parameters of the liquid film beyond this limit. The spread of the film over the surface of the heater depends on the distance L from the source of jets to the surface of the target. So, for the case $L = 10.5$ mm (the distance between the centers of jet impacts is $l = 1.34$ mm), the liquid film spreads only over part of the working surface (Fig. 8a). For the case $L = 35.5$ mm and $l = 4.52$ mm (Fig. 8b), the film spreads over the entire surface. For $L = 80.5$ mm and $l = 10.24$ mm (Fig. 8c), the centers of

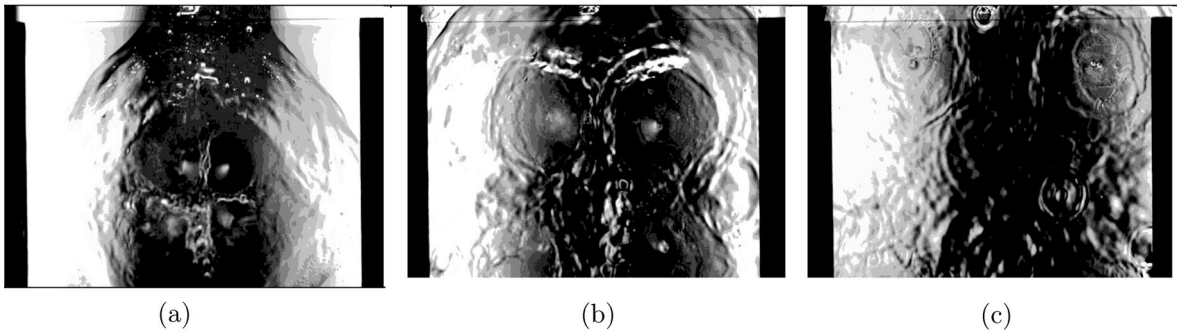

Fig. 8. Results of water spread pattern on working surface. Liquid flow rate: 8.23 g/s ($\Delta p = 3$ atm). Heat flux density $q = 51.5$ kW/m^2. Distance from the liquid source: (a) $L = 10.5$ mm; (b) $L = 35.5$ mm; (c) $L = 80.5$ mm.

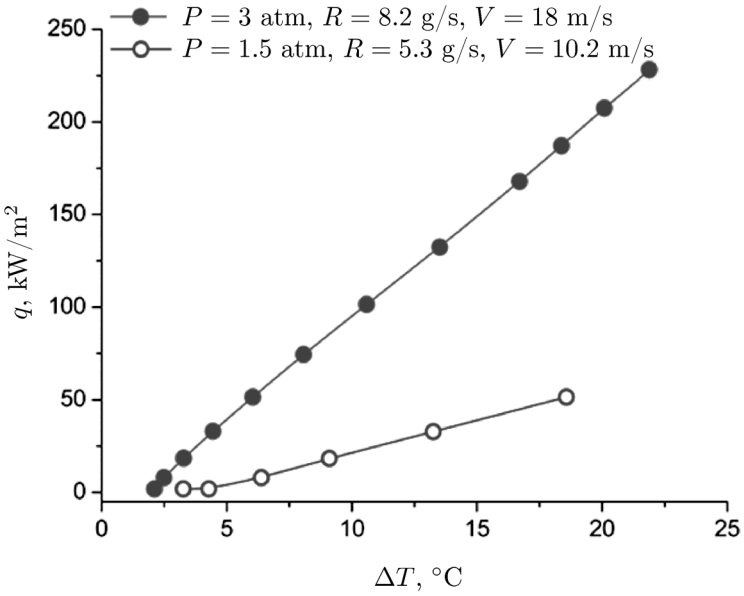

Fig. 9. Heat flux density vs. degree of overheating of heat-generating surface at jet watering for different P values at nozzle inlet ($L = 30.5$ mm).

jet impacts are located in the corners of the working surface. Basically, the liquid film spreads over the entire surface, but in its central part there may appear short-term ruptures of the film with subsequent watering over the local dry area.

For $L = 10.5$ mm and $L = 35.5$ mm, the film structure between the centers of jet impacts has a complex three-dimensional surface resembling rivulets. This is due to the interaction of the flow of the liquid film from the jets, spreading due to the kinetic energy of the jet and the force of gravity. The shape of these hydraulic ripples depends on the distance L (see Figs. 8a and 8b). No such film structure is observed at $L = 80.5$ mm.

HEAT TRANSFER

Figure 9 shows the heat flux density q against the superheating degree of the surface ΔT for two pressure values: $\Delta p = 1.5$ atm (flow rate $G = 5.4$ g/s, jet velocity $V_0 = 10.5$ m/s) and 3 atm ($G = 8.3$ g/s, jet velocity $V_0 = 16.5$ m/s) at the nozzle inlet at $L = 30.5$ mm. The experimental data show a linear dependence of the heat flux density on the surface superheating.

Figure 10 demonstrates the gradient temperature fields obtained with the IR camera in the regimes of interaction of the jets with the heating surface shown in Fig. 8.

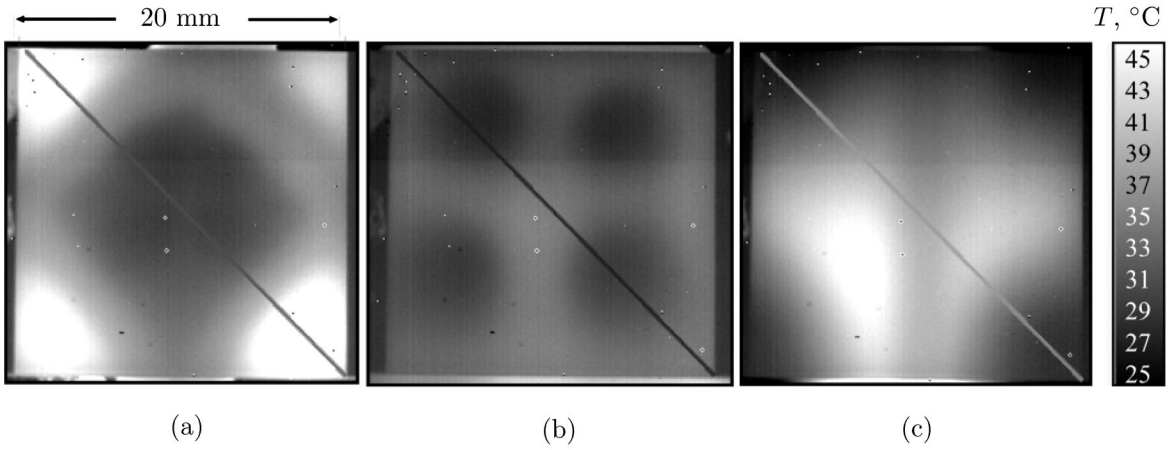

Fig. 10. Frames of IR thermography of temperature field of heating surface at multi-jet irrigation at different distances from source: (a) $L = 10.5$ mm; (b) $L = 35.5$ mm; (c) $L = 80.5$ mm ($\Delta p = 3$ atm, $q = 51.5$ kW/m^2).

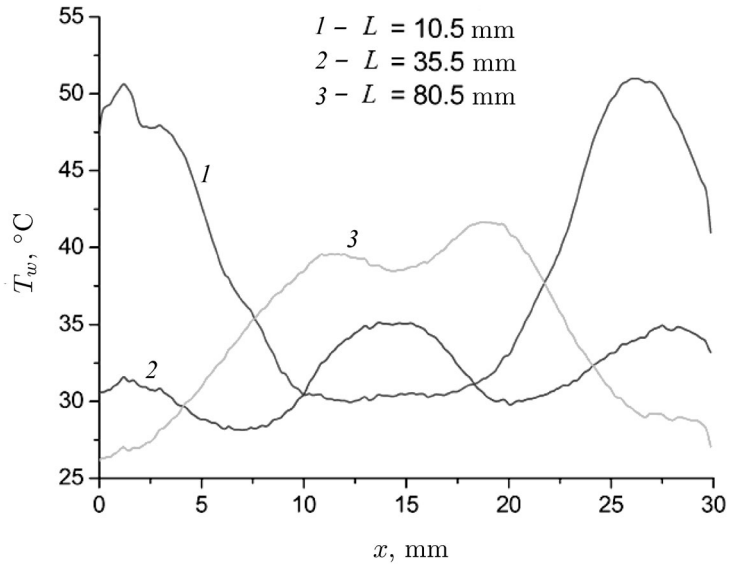

Fig. 11. Temperature distribution on heating surface at multi-jet irrigation along lines shown in thermograms (Fig.10).

It is clear from the presented frames that the temperature field is non-uniform. The lowest temperature corresponds to the areas located at the point of impact of the jets.

Figure 11 displays the temperature distribution along the lines (see Fig. 10) in the described regimes. The temperature profiles have a more complex distribution structure than in the case of single jets. This is due to the interaction of neighboring jets. The temperature profiles (Fig. 11) show that the low-temperature surface regions correspond to the jet impact areas. At $L = 10.5$ mm (Fig. 11, curve *1*), the distance between the four jets is small ($l = 1.34$ mm). In this regime, the temperature field of the surface to the four jets is equivalent to the influence of a single jet [7–9]. At $L = 10.5$ mm and 80.5 mm, each jet of the array forms a cell, which has in its jet flow zone a stagnation zone and adjacent radial zones of the film flow. The temperature profiles of these regimes have a wave-like shape with minima in the areas of jet impacts. The local heat transfer at the site of interaction of each jet from the array can be considered as heat transfer to a single jet. The heat transfer in the space between the jets depends on the interaction of the liquid film propagating from the jet impact on the surface and the force of gravity. Thus, for $L = 80.5$ mm (Fig. 11, curve *3*), a local temperature minimum is observed in the interval from 10 mm

to 20 mm. This minimum corresponds to the flow of the liquid film, the structure of which is formed by the jets upon the impact to the heat-transfer surface.

Figure 12a shows the dependence of the Nusselt number of a single jet against the distance L from the source to the surface. The Nusselt number is calculated by the following formula [10]:

$$Nu_d = \frac{\alpha \cdot d_{jet}}{k_f},$$

where d_{jet} is the jet diameter on the heat transfer surface bounded by a hydraulic ripple (Figs. 12b and 12c); k_f is the coefficient of thermal conductivity of the liquid at room temperature; the heat transfer coefficient α [W/(m^2·K)] was determined by the following formula:

$$\alpha = \frac{q}{T_{sj} - T_{jet}}.$$

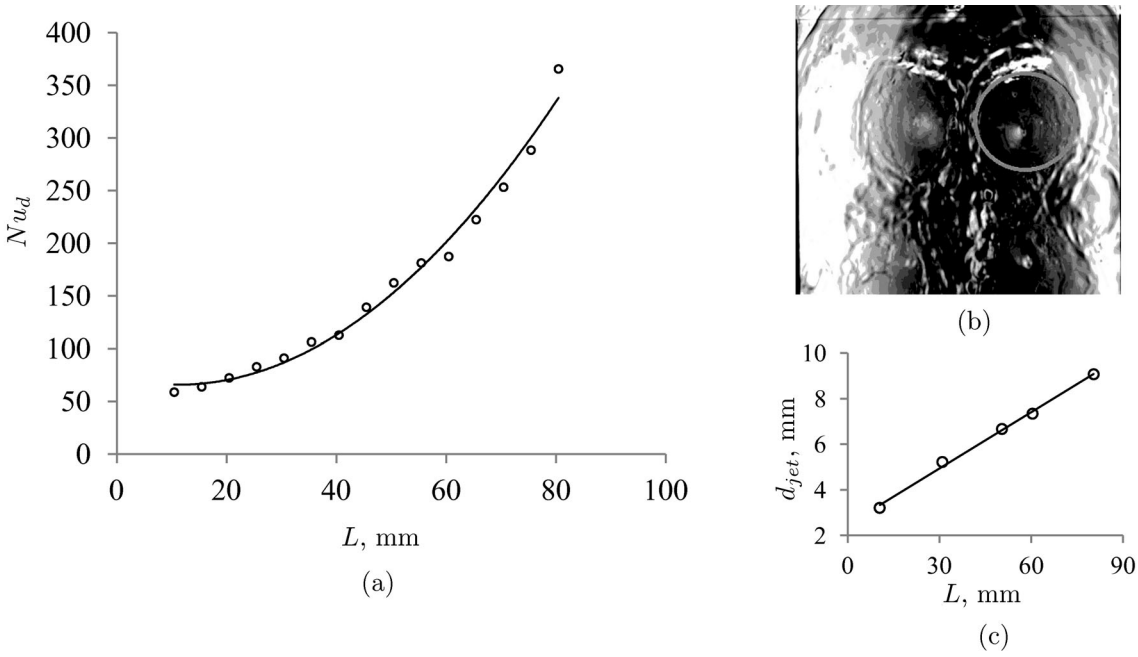

Fig. 12. (a) Nusselt number of single jet at nozzle inlet pressure $P = 3$ atm; (b) determination of jet diameter d_{jet} on heat transfer surface, (c) jet diameter at impact to surface vs. L.

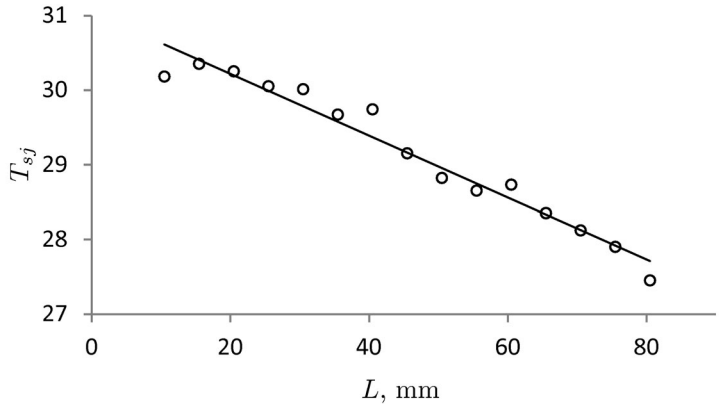

Fig. 13. Mean temperature of heat transfer surface under jet (see Fig. 12b) vs. distance from source.

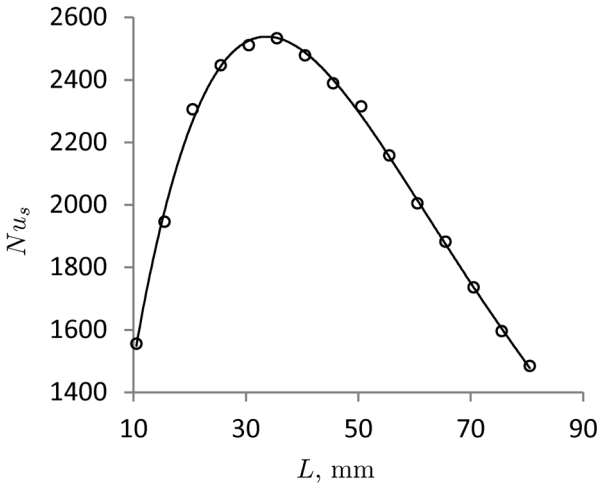

Fig. 14. Integral Nusselt number vs. distance from source at nozzle inlet pressure $P = 3.5$ atm.

Here q is the heat flux density [W/m^2]; T_{sj} is the average surface temperature in the jet area bounded by the hydraulic ripple (see Fig. 12b); T_{jet} is the jet (room) temperature.

The curve of the Nusselt number of a single jet exponentially grows. This is due to the decrease in the difference between the surface temperature T_{sj} under the jet (see Fig. 12b) and the liquid jet temperature T_{jet}. Figure 13 shows the experimental data for the mean temperature T_{sj} versus the distance L.

Figure 14 shows the dependence of the integral Nusselt number for the entire surface on L at the nozzle inlet pressure $P = 3$ atm. The integral Nusselt number was calculated by the following formula:

$$Nu_s = \frac{\alpha \cdot l_s}{k_f},$$

where l_s is the heater length.

The curve is bell-shaped, which is consistent with results of other authors [10–13]. The figure shows that the maximum heat transfer coefficient corresponds to $L = 35.5$ mm and $Nu_s = 2532$. In our case, the velocity of the liquid jets at the heat transfer surface decreases slightly depending on the distance from the source to the target. So, the decisive factor affecting the heat transfer is the distribution of the centers of jet impacts on the surface. The heat transfer is maximal when the area of the liquid film around the centers of the jet impacts, which has a smaller thickness and a higher flow velocity than the liquid film on other parts of the working surface, is distributed over a larger heat transfer area.

CONCLUSIONS

Characterization of the droplet jet of water formed by the Bosch EV14L nozzle was performed by the shadow technique. Data of the distribution of the droplet diameters and their velocity against the nozzle inlet pressure were obtained. A measurement method based on synchronized high-speed infrared thermography and video recording was used to study the temperature field in relation to the process of formation and behavior of precipitated liquid on the heated surface. The distribution of the centers of jet impact to the surface depends on the distance from the source. Around the jet impact centers, a film structure is visible with the border in the form of hydraulic ripple. In the zone of deceleration, beyond the hydraulic ripple, the film structure has a complex three-dimensional surface resembling rivulets.

It has been demonstrated that the heat transfer coefficient in non-boiling regime at multi-jet cooling is unequally spatially distributed value over the heater surface. For example, the temperature in the region of the impact droplet jet is much lower than in other areas of the heater. It is shown that the heat transfer coefficient depends on the distance from the spray source to the heating surface during stationary irrigation. The optimal distance with the maximum heat transfer coefficient has been determined for a given configuration of irrigation points relative to the heating surface of a given area.

FUNDING

This work was supported by Program of Fundamental Scientific Research of the Russian Academy of Sciences for 2013–2020 (theme III.18.2.3, AAAA-17-117030310025-3) and by Russian Foundation for Basic Research and the government of the Novosibirsk region of the Russian Federation, project no. 18-48-540018.

REFERENCES

1. Liang, G. and Mudawar, I., Review of Spray Cooling—Part 1: Single-Phase and Nucleate Boiling Regimes, and Critical Heat Flux, *Int. J. Heat Mass Transfer*, 2017, vol. 115, pp. 1174–1205.
2. Smakulski, P. and Pietrowicz, S., A Review of the Capabilities of High Heat Flux Removal by Porous Materials, Microchannels and Spray Cooling Techniques, *Appl. Therm. Eng.*, 2016, vol. 104, pp. 636–646.
3. Chunqiang, S., Shao, S., Changqing, T., and Hongbo, X., Development and Experimental Investigation of a Novel Spray Cooling System Integrated in Refrigeration Circuit, *Appl. Therm. Eng.*, 2012, vol. 33, pp. 246–252.
4. Serdyukov, V.S., Surtaev, A.S., Pavlenko, A.N., and Chernyavskiy, A.N., Study on Local Heat Transfer in the Vicinity of the Contact Line under Vapor Bubbles at Pool Boiling, *High Temp.*, 2018, vol. 56, no. 4, pp. 546–552.
5. Surtaev, A., Serdyukov, V., Zhou, J., Pavlenko, A., and Tumanov, V., An Experimental Study of Vapor Bubbles Dynamics at Water and Ethanol Pool Boiling at Low and High Heat Fluxes, *Int. J. Heat Mass Transfer*, 2018, vol. 126PB, pp. 297–311.
6. Gerardi, C., Buongiorno, J., Hu, L.W., and McKrell, T., Study of Bubble Growth in Water Pool Boiling through Synchronized, Infrared Thermometry and High-Speed Video, *Int. J. Heat Mass Transfer*, 2010, vol. 53, no. 19, pp. 4185–4192.
7. Stevens, J. and Webb, B.W., Measurements of the Free Surface Flow Structure under an Impinging, Free Liquid Jet, *J. Heat Transfer*, 1992, vol. 114, no. 1, pp. 79–84.
8. Garimella, S.V. and Rice, R.A., Confined and Submerged Liquid Jet Impingement Heat Transfer, *J. Heat Transfer*, 1995, vol. 117, no. 4, pp. 871–877.
9. Gao, N. and Ewing, D., Investigation of the Effect of Confinement on the Heat Transfer to Round Impinging Jets Exiting a Long Pipe, *Int. J. Heat Fluid Flow*, 2006, vol. 27, pp. 33–41.
10. Robinson, A.J. and Schnitzler, E., An Experimental Investigation of Free and Submerged Miniature Liquid Jet Array Impingement Heat Transfer, *Exp. Therm. Fluid Sci.*, 2007, vol. 32, pp. 1–13.
11. Pan, Y. and Webb, B.W., Heat Transfer Characteristics of Arrays of Free-Surface Liquid Jets, *J. Heat Transfer*, 1995, vol. 117, pp. 878–883.
12. Yonehara, N. and Ito, I., Cooling Characteristics of Impinging Multiple Water Jets on a Horizontal Plane, *Techn. Rep. Kyushu Univ.*, 1982, vol. 24, pp. 267–281.
13. Jiji, L.M. and Dagan, Z., Experimental Investigation of Single-Phase Multijet Impingement Cooling of an Array of Microelectronic Heat Sources, in *Cooling Technology for Electronic Equipment*, Aung, W., Ed., Washington, DC: Hemisphere Publ., 1988, pp. 333–351.